Fabrication of Ultra-Thin Suspended Membranes from Atomic Layer Deposition Films

Running title: Ultra-Thin Suspended Membranes from ALD Films

Running Authors: Elowson et al.

Michael J. Elowson[1,a)], Rohan Dhall[1], Adam Schwartzberg[1], Stephanie Chang[1], Vittoria Tommasini[1], Sardar B. Alam[1,2], Emory M. Chan[1,2], Stefano Cabrini[1] and Shaul Aloni[1]

[1]The Molecular Foundry, Lawrence Berkeley National Laboratory, 1 Cyclotron Rd, Berkeley, CA 94720
[2]Materials Sciences Division, Lawrence Berkeley National Laboratory, 1 Cyclotron Rd, Berkeley, CA 94720

[a)] Electronic mail: melowson@lbl.gov, elowson19@gmail.com

ABSTRACT

Ultra-thin films suspended as freestanding membranes are critical to many microelectronic and materials science applications. However, fabrication methods are currently limited in either their flexibility, due to material selectivity issues during the final membrane release, or their scalability. Here, we demonstrate a novel fabrication process for suspending ultra-thin films with thicknesses as low as 4 nm and lateral dimensions up to 20 x 1000 μm from a variety of materials grown by atomic layer deposition. A silicon nitride membrane serves as support for a sacrificial polymer layer and an ultra-thin atomic layer deposition film which, after plasma etching, will form the membrane. The high chemical selectivity between atomic layer deposition-grown transition metal nitrides and oxides and the sacrificial polymer means that ultra-thin films of a variety of materials can be released without damage using a single process. Electrically conductive titanium nitride membranes can be produced by this method and are of significant interest for electron

microscopy applications. Electron transparency of titanium nitride membranes was found to be ~14% higher than silicon nitride of the same thickness, and of similar conductivity to graphite, meaning that ultra-thin, conductive, and electron transparent membranes can be fabricated at scale. These membranes are ideal supports for electron and photon characterization techniques, as well as microelectromechanical systems applications that require a conductive membrane.

I. INTRODUCTION

Ultra-thin (<100 nm) suspended membranes find use in a wide variety of microelectronic and materials science applications, including sensors,[1-3] filters,[4] micro-fuel cells,[5] and sample supports,[6] where they serve as barriers which may be only several to hundreds of atoms thick. Many electron and photon characterization techniques benefit from such ultra-thin sample supports, or "windows," which minimize scattering of the incident radiation and thereby improve the signal-to-noise ratio from the sample of interest.[7]

Ultra-thin membranes are often fabricated using techniques that have been standardized by the semiconductor and microelectromechanical systems (MEMS) industries, allowing for scalable production.[8] Microfabrication of a suspended membrane is performed by growth or deposition of the membrane film on a substrate, followed by removal of the support materials under it to yield a free-standing structure. Since the membrane film is several orders of magnitude thinner than the substrate, it is very fragile in comparison. Therefore, the ability to release such a film without damage requires a

highly selective process that effectively removes the substrate, but has minimal effect on the membrane material.

For example, silicon-rich silicon nitride (SiN) is the most common material for microfabricated ultra-thin membranes, favored for its low tensile stress, mechanical robustness, and simple and inexpensive fabrication.[6] The simple fabrication of SiN membranes is enabled by the very high selectivity of low pressure chemical vapor deposited (LPCVD) SiN to silicon in potassium hydroxide (KOH) etching, estimated to range from approximately 1:30,000 to 1:50,000.[9] This high level of selectivity is required to release ultra-thin membranes without damage, but only a limited number of material combinations offer it. Therefore, the fabrication process often needs to be designed specifically around the issue of material selectivity; i.e., the membrane material is limited by its resistance to the etch process used to release it.

More recently, two-dimensional materials such as graphene,[10] hexagonal boron nitride,[11] and molybdenum sulfide[12] have been suspended as atomically thin membranes which offer unique material properties. However, these two-dimensional materials are not yet compatible with standard fabrication techniques, meaning they cannot be suspended using scalable methods. Rather, the films must be isolated separately and manually transferred onto a perforated support, which often results in folds, wrinkles, and adhesion issues that limit their usable area and reproducibility.[6]

By solving this issue of material selectivity, and doing so with scalable methods, one could make ultra-thin membranes from a much wider variety of materials, enabling membrane-based sensors, filters, or sample supports with customizable properties. For

example, electrical or thermal conductivity, surface chemistry, optical and/or electron transparency, etc. can be tuned based on the needs of the application.

Atomic layer deposition (ALD) is an increasingly prominent technique capable of depositing a wide variety of ceramic materials with exceptional quality using self-limiting growth.[13,14] Even down to several nanometers in thickness, ALD films are uniform, conformal, and pinhole-free.[15] ALD can also be used to conveniently alternate nanoscale films of two or more materials, creating composites or "nanolaminates" which are amongst the strongest materials ever synthesized.[16] Nanolaminates offer a high level of customizability based on the materials selected and arrangement of the films. Materials can be arranged such that the beneficial properties of each are well-utilized. Additionally, nanolaminates can be tuned to exhibit unique physical traits as the layer thickness becomes less than or equal to the length scale that defines the property.[17-19]

ALD offers the flexibility, precision, and film quality necessary for ultra-thin membrane applications, including electron-transparent windows,[20-23] metamaterials,[24] tynodes,[25-27] nanopores,[28-30] solid-oxide fuel cells,[31-33] insulating layers,[34,35] and mechanical studies.[36-39] Though these applications successfully use ALD films as suspended structures, they are all limited in their fabrication by either material selectivity or scalability. Specifically, most of these reports use a fluorine-based dry etch process as the final release step, limiting the membrane material to one which is chemically resistant to fluorine. Other reports use suspended graphene or amorphous carbon as a support layer onto which the ALD film is deposited, requiring a manual transfer of the support layer before the ALD film can be deposited. This process is not scalable.

In this work, we introduce a novel fabrication process which yields ultra-thin membranes from a variety of ALD materials using a single flexible and scalable process. By utilizing a sacrificial polymer, we introduce a high level of selectivity in the final membrane release step. The polymer is etched using a low power oxygen plasma, which many transition metal nitrides and oxides are resistant to.[40] Therefore, a wide variety of ALD-grown ceramics can be released as ultra-thin membranes with high yield, without the need to perfect the final release etch or tune it to the specific material being released. The flexibility and precision of ALD, coupled with the ability to combine multiple materials to form nanolaminates, allow for membranes with tunable properties that can be highly-customized to the needs of the application.

We demonstrate membranes ranging from 4 to 55 nm in thickness, with lateral dimensions up to 20 x 1000 μm. We focus here on titanium nitride (TiN) as our initial material of interest due to its electrical conductivity,[41] low atomic number, hardness,[42] corrosion resistance,[43] and biocompatibility.[44]

II. EXPERIMENTAL

A. Silicon Nitride Windows

SiN membranes, or "windows," serve as a scaffold for the creation of a new membrane in subsequent steps and were made using well-established microfabrication methods.[45-47]

The fabrication, summarized in Fig. 1, was carried out on 200 μm-thick, double-side polished silicon wafers coated with 50 nm of low-stress (<250 MPa) LPCVD SiN.

Photolithography was used to pattern rectangular geometries on the wafer backside, and reactive ion etching was used to transfer the pattern from the photoresist to the SiN, using CHF_3 (CAS# 75-46-7, 99.999% purity from AirGas USA) and O_2 (CAS# 7782-44-7, 99.993% purity from Praxair Technology) gas chemistry with a 48/2 sccm CHF_3/O_2 ratio, 55 mTorr of pressure, 20°C as the table temperature, and 25 W of forward power in an Oxford System 80+ Reaction Ion Etcher (RIE). The SiN etch rate was measured via ellipsometry and found to be approximately 9 nm/min. The patterned backside SiN then served as a mask for etching through the silicon substrate in 30% KOH (CAS# 1310-58-3, ≥85% purity pellets from Sigma-Aldrich) solution heated to 80°C, which etched the silicon at approximately 80 μm/hr. The silicon substrate was etched along the [111] crystal planes to create inverse-pyramid trenches sloping at 54.7°. Where the patterned geometries were large enough, the KOH etched all the way through the silicon until it reached the SiN on the opposite face of the wafer, forming rectangular SiN membranes. Where the geometries were not large enough, the silicon etching self-terminated as the [111] planes met either along a straight line or at a single point. Long, narrow rectangular geometries were used to create V-shaped grooves in this way, thinning the silicon along these lines for cleaving into smaller pieces and individual chips. See Fig. 1(a).

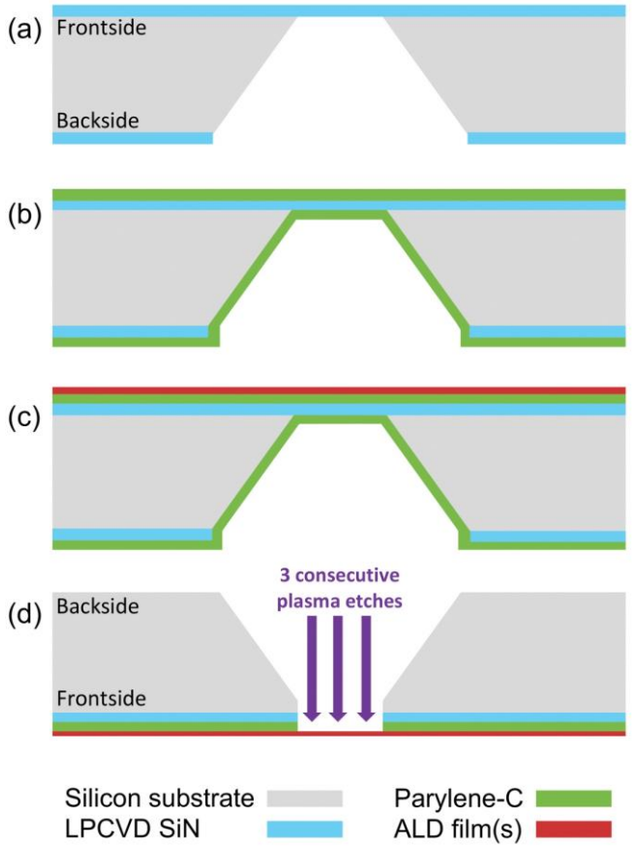

FIG. 1. A simplified fabrication process flow. (a) Fabricate SiN windows using standard methods, (b) deposit the sacrificial polymer, which in the case of Parylene-C coats both sides of the wafer, (c) deposit the membrane material of choice via ALD, and finally (d) plasma etch the support materials from the backside. Not shown: protective polymethyl methacrylate spin coating after (c) and removal in dichloromethane after (d).

B. Deposition of Sacrificial and Membrane Materials

The SiN windows then served as a base from which to fabricate the ALD-based membranes. The simplest possible process would be to deposit the ALD film directly on the SiN window, then etch the SiN from the backside via reactive ion etching to release the membrane. However, physical bombardment from the ions can easily create pinholes,

cracks, or tears in an ALD film of only a few nanometers in thickness. Avoiding any ion bombardment of the ALD film from over-etching the SiN would require a very uniform etch, with a very accurate measure of the SiN thickness and etch rate.

Therefore, another sacrificial layer was introduced, Parylene-C, as it can be removed with high selectivity to ALD-grown ceramics using a low power oxygen plasma, with little consequence to over-etching. Furthermore, a dry etch process allows one to avoid immersion of fragile membranes in a liquid etch bath, increasing the likelihood that the membranes stay intact through the final release step.

Parylene-C not only provides high selectivity, but is also insoluble in typical cleanroom solvents. A polymer that dissolves or delaminates in solvents would otherwise lift-off the ALD layer and ruin the membrane during any cleaning. Parylene's resilience in liquids also allows for subsequent lithography steps to be conducted, for instance to pattern metal electrodes or the membrane film itself, as lithography typically requires immersion in a solvent or base for resist development.

Furthermore, Parylene is deposited in the gas phase using the Gorham Process,[48] a gas-phase chemical vapor deposition process which conformally coats all surfaces and is less likely to break the SiN windows compared to a liquid-based coating process. Therefore, Parylene coats both sides of the wafer, and importantly both sides of the SiN windows as shown in Fig. 1(b). Parylene-C was deposited from di-chloro-di-p-xylylene dimer (CAS# 28804-46-8, >90% purity from Specialty Coating Systems). Depositions ranged from 180 to 300 nm in thickness, measured via profilometry.

Following Parylene deposition, the membrane material of choice was then deposited at the desired thickness by ALD. There is great flexibility in the membrane

material, as most ALD materials are ceramics which are highly resistant to oxygen plasma. ALD also allows one to conveniently deposit multiple films in a variety of arrangements, with very precise control over each film's thickness.

ALD depositions were conducted in an Oxford FlexAl Plasma-Enhanced ALD, with deposition parameters dependent on the material and deposition temperature (details on process parameters and precursor chemistries given in Supplemental Material). Growth rates were determined by ellipsometric measurements, which were used to calculate the thickness of the ALD films, and therefore the released membranes, based on the number of deposition cycles. Thickness of the TiN films grown by ALD ranged from 4 to 55 nm.

As a polymer, Parylene-C has a limited thermal budget, with a melting temperature of 290°C.[49] Though previous reports have indicated that Parylene-C can be safely annealed for several hours at 300°C,[50] we limited our depositions to 100°C to protect the cleanliness and vacuum level of the ALD chamber. However, other variants of Parylene such as Parylene F and AF-4 are stable at higher temperatures,[51,52] and these variants could potentially be substituted into the process to allow for ALD depositions at 300°C for increased film crystallinity,[53] hardness, and elastic modulus.[54]

Deposition of the membrane material via ALD resulted in a stack of thin films built from the SiN windows. Under the ALD membrane material was the frontside layer of Parylene-C, the SiN, and finally the backside layer of Parylene-C, as shown in Fig. 1(c).

C. Membrane Release via Backside Etching

To release the membrane, the three support layers were removed via a sequence of reactive ion etches. These etches must be selective enough to fully remove their intended support material, while leaving no residues and minimizing any damage to the ultra-thin ALD film.

The etches were conducted in an Oxford System 80+ RIE. Because the samples lie face down in the RIE, 495 PMMA A6 electron-beam resist from MicroChem Corp. was first spun on the top surface at 2000 rpm, leaving a protective layer of polymethyl methacrylate (PMMA) approximately 400 nm in thickness. The PMMA was baked in a convection oven at 110°C for 30 minutes. Because this PMMA layer is not patterned, uniformity of the resist is less important and therefore a bake temperature lower than the recommended temperature of 170°C was acceptable.

In the RIE, the backside layer of Parylene-C was first etched using a low power oxygen plasma. The recipe uses 50 sccm of O_2, 80 mTorr of pressure, 20°C as the table temperature, and 20 W of forward power. The etch rate was measured via profilometry and found to be approximately 20 nm/min. However, Parylene residues were leftover even after over-etching by 50%. Therefore, extended etches were used to ensure that all Parylene residues were removed. Considerations on residues and over-etching will be discussed in more detail in the next section.

Next, the LPCVD SiN layer was etched using CHF_3/O_2 gas chemistry with a 48/2 sccm ratio, 55 mTorr of pressure, 20°C as the table temperature, and 50 W of forward power. It was found that increasing the forward power from 25 to 50 W did a significantly better job in preventing SiN residues. The etch rate was found to be

approximately 17 nm/min, however a 100% over-etch was used to ensure that all residues were thoroughly removed.

Finally, the frontside layer of Parylene-C, which is directly under the ALD layer, was etched using the aforementioned oxygen plasma recipe, and was also over-etched to prevent residues. Because this is the final etch step in releasing the membrane, this etch is where the high selectivity and gentle processing are critical in minimizing damage such as pinholes, cracks, or tears in the ultra-thin ALD layer.

The resulting membranes were composed of the ALD layer with the protective PMMA still on the surface. Before use, the samples were cleaved into individual chips and submerged in dichloromethane (CAS# 75-09-2, ≥99.5% purity from Macron Fine Chemicals) for 30 sec to remove the PMMA, followed by dips in acetone (CAS# 67-64-1, ≥99.3% purity from J.T. Baker) and isopropanol (CAS# 67-63-0, ≥99.9% purity from MilliporeSigma) to promote a clean surface. The ALD film was then completely isolated as an ultra-thin membrane, as illustrated in Fig. 1(d). Scanning electron microscope (SEM) images of a finished membrane are shown in Fig. 2.

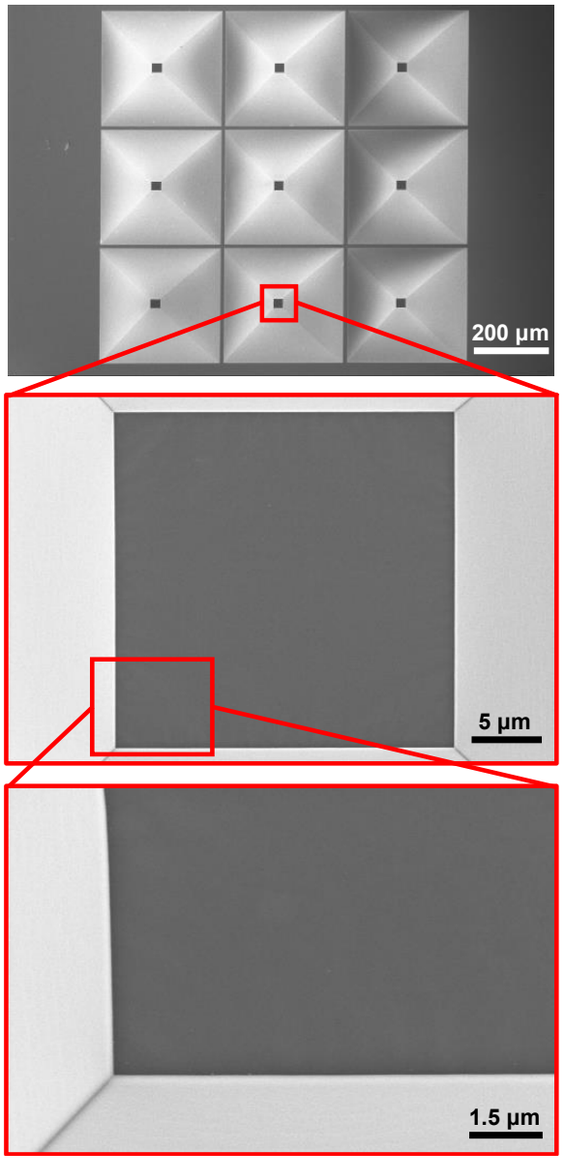

FIG. 2. A finished TiN membrane, approximately 8 nm in thickness with lateral dimensions of 20 x 20 µm, imaged from the backside. The release etches were optimized to give a clean membrane surface with no residues. Membrane thickness was calculated from ALD deposition rates that were measured via ellipsometry. TiN films deposited at 100°C were measured to be approximately as conductive as graphite.

D. Characterization via EDX, EELS, and Four-Point Probe

Finished membranes were imaged and characterized using energy-dispersive x-ray spectroscopy (EDX)[55] in a Zeiss Gemini Ultra-55 Analytical SEM equipped with a Bruker Quantax EDX detector. Images were also taken in a Zeiss Ultra-60 SEM.

Energy filtered transmission electron microscopy (TEM) and scanning TEM (STEM) were performed on a monochromated FEI Tecnai microscope equipped with a Gatan Imaging Filter.

Sheet resistivity of the ALD-grown films was measured using a Four Dimensions 120 HH four-point probe in a low pre-amp gain mode. Four-point probe data is presented in the Supplemental Material.

III. RESULTS AND DISCUSSION

A. Optimization of Final Backside Etches

Successful fabrication of a suspended membrane requires that the membrane film is properly released without damage. Specifically, the support materials must be fully removed with minimal residues leftover. Achieving this requires that the final etches are optimized such that they fully remove their intended material, but are simultaneously selective and gentle enough to not damage the membrane film.

To optimize these etches, characterization of the etch rate via ellipsometry or cross-section imaging was not sufficient, as they did not capture the possibility for residues leftover on the surface. Therefore, the backsides of the chips and membranes were inspected before and after each etch step by SEM. Parameters such as etch time and forward power were varied to determine their effect on the leftover residues from each support material.

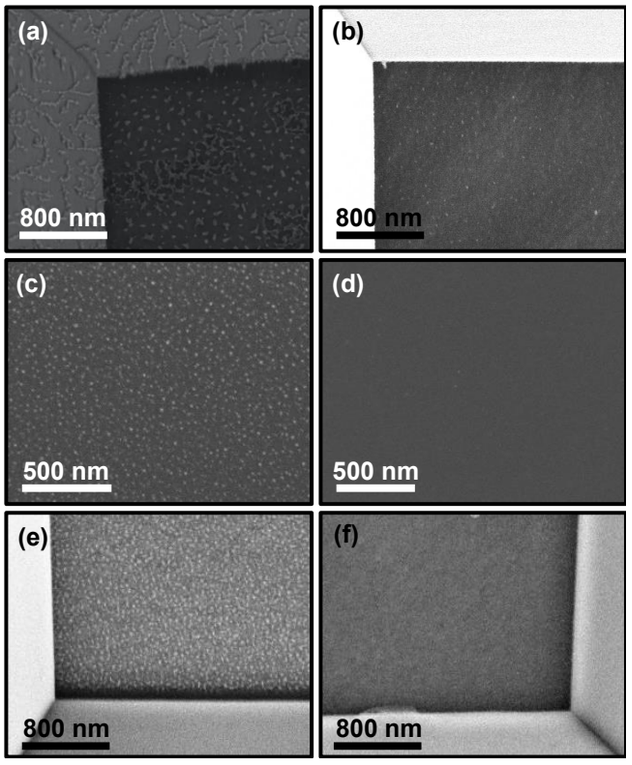

FIG. 3. Optimizations for backside RIE etches. (a) Partial backside ALD coverage, (b) addressed via larger borders and better contact with carrier wafer. (c) Incomplete SiN removal at 25 W of forward power, (d) addressed by increasing to 50 W. (e) Parylene residues leftover even with 50% over-etch, (f) addressed by using a 200% over-etch.

A consistent source of residues on the backside of the membranes was not a result of incomplete etches, but rather a partial backside coverage from the ALD deposition. As a conformal deposition method, ALD precursors are able to diffuse through small gaps between the sample and carrier wafer and partially coat the back surface. Even in areas far from any visible border, this can create a web-like network of partial ALD coverage. This backside coverage masks the other etches, meaning the support materials are not removed in these covered areas. However, because the ALD layer is so thin, there is not

enough texture or contrast to see this backside coverage via SEM until after the first Parylene etch, shown in Fig. 3(a).

This issue was sufficiently addressed by depositing on samples with larger borders around the individual window chips, and by using new, clean carrier wafers to promote better contact. However, future work will include fabrication of a custom carrier that can seal the edges of the substrate in order to prevent this backside coverage.

It was also found that our standard SiN etch recipe was not sufficient for a residue-free removal of SiN. We hypothesize that this is not noticeable when making SiN windows, because the KOH solution can still easily access the silicon and etch through the wafer. We found that doubling the forward power from 25 to 50 W did an excellent job at eliminating SiN residues, as shown in Fig. 3(d), even when the etch time was lowered to compensate for the difference in etch rate.

Finally, EDX was used to characterize the final release etch on finished 55 nm thick TiN membranes. To determine whether the support materials were fully removed, particularly the final layer of Parylene, measurements were taken from the front and back membrane surfaces and compared for various etch durations. It was assumed that if the amount of carbon detected on the front and back surfaces of the membranes were equal, the final Parylene layer was fully removed. This could also be verified visually in the SEM to confirm a lack of residues. Measuring zero carbon to confirm complete Parylene removal is not feasible, as there is always some carbon impurity in the ALD film and adhered to the surface from exposure to atmosphere.

EDX is not particularly surface-sensitive, however the acceleration voltage of the electron beam was minimized to balance adequate signal and x-ray generation with

surface sensitivity. Measurements were taken at 2 kV, which for TiN results in an estimated interaction depth of 60 nm.[56] Measurements were taken on chips that underwent between 13.5 and 81 minutes of final Parylene etching, representing a 50% to 800% over-etch for a 180 nm thick Parylene layer etched at 20 nm/min.

X-ray photoelectron spectroscopy (XPS)[57] is highly surface-sensitive due to its low interaction depth, and therefore may be more appropriate for these measurements. However, XPS was not used here because the available system's electron detector is placed at an angle such that there is no signal from the bottom of the 54.7° sloped trench where the back surface of the membrane is found. The larger x-ray spot size in XPS also makes it difficult to measure only the membrane area without the inclusion of other areas such as the trench. However, future work will include angle-resolved XPS measurements on larger windows using a tilted sample holder.

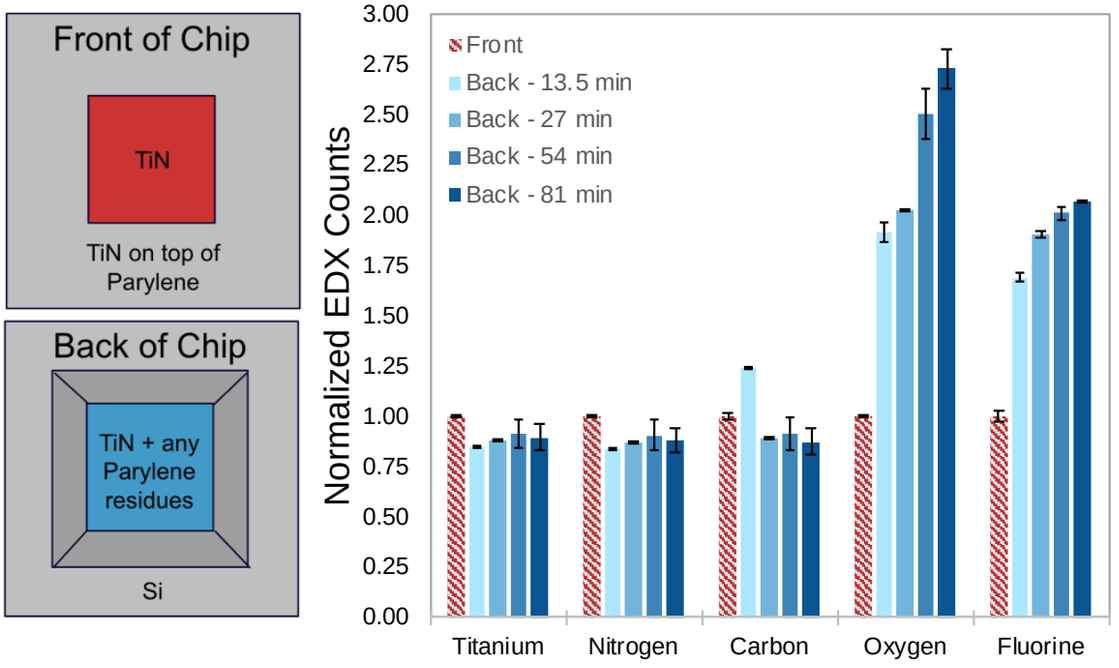

FIG. 4. Normalized EDX signal for elements of interest taken from the front and back surfaces of a 55 nm thick TiN membrane. For each element, EDX counts are normalized to the average signal measured from the front surface for that element. Back surfaces were measured after various durations of the final Parylene etch, and the relative amount of signal for each element can be tracked as the duration of etching increases. At 13.5 min, there is excess carbon, suggesting incomplete Parylene removal. From 27 min onward, the carbon level on the back surface is lower than that from the front surface and stays consistent, but oxidation and fluorination increase from extended exposure to reactive species in the RIE chamber.

Figure 4 shows the chemical signals measured by EDX for various durations of the final etch. For each element, EDX counts are normalized to the average signal measured from the front surface for that element. The relative amount of these chemical species on the back surface can be tracked as the duration of etching increases and compared to the signal from the front surface. A carbon signal less than or equal to that

from the front surface suggests that the final Parylene layer has been fully removed and the surface has gone from under- to over-etched. At 13.5 min of etching there is a higher level of carbon on the back surface compared to the front, suggesting that there is still Parylene present. Visible residues on this sample are also shown in Fig. 3(e). The 27 min etch represents a 200% over-etch and the resultant level of carbon on the back surface is slightly lower than the front. As the length of final etching increases to 54 and finally 81 minutes, the level of carbon stays consistent, but oxidation and fluorination on the back surface increase. This is due to the extended exposure of the back surface to oxygen plasma. The increase in fluorination may be due to leftover fluorine in the RIE chamber from the SiN etch, as vacuum is not typically broken between the final etch steps. In general, the slightly lower signal for titanium, nitrogen, and carbon from the back vs. the front surfaces may be a result of the trench from which the emitted x-rays must escape. For the flat front surface there is a more direct path between the scan area and the detector.

The similar levels of carbon measured on the front and back surfaces after 27 min, coupled with the lack of residues imaged by SEM, suggest a complete removal of the support materials and successful release of the membrane. Therefore, it was determined that a 200% over-etch in the final etch step is sufficient in removing all Parylene, though there is excess oxidation and fluorination of the back surface. A 100% over-etch was also used for later fabrication batches, with similar success, but was not characterized with EDX.

Through the development of the fabrication process, it became apparent that over-etching was necessary at each step in order to eliminate residues from the back surface of

the membrane. The ability to over-etch each support layer, even to drastic levels, is made possible by the combination of support materials used and their selectivity during each etch step. Specifically, Parylene can be heavily over-etched with an oxygen plasma without damaging the SiN or ALD layers. SiN can be over-etched at higher powers, with enough selectivity to Parylene to not etch through the final support layer. This is representative of the flexibility and convenience that this fabrication process allows. Ultra-thin membranes of a variety of materials can be realized without the need to perfect the final release etch or tune it to the specific material being released.

B. Electron Transparency by EELS

TiN membranes 10 nm in thickness were imaged by STEM using a 200 kV beam acceleration voltage. The TiN layer was observed to be nanocrystalline by electron diffraction imaging, with very limited diffraction observed through the membrane, thus suggesting the suitability of its nanostructure as a TEM sample support. The membrane was also stable throughout prolonged exposure to the electron beam with a dose typical for bright field TEM imaging (~100 $e \cdot Å^{-2} \cdot s^{-1}$).

A spatial thickness map was taken using electron energy loss spectroscopy (EELS) over an approximate area of 300 x 300 nm on the membrane, shown in Fig. 5(a). Brighter areas represent bits of contamination on the membrane, where the thicker material results in more high-angle electron scattering, and darker areas represent the TiN membrane itself. A rectangular profile was taken across one area of contamination, and the intensity of transmitted electrons that do not lose energy (zero-loss) is compared to the total transmitted intensity using the "log-ratio" formula:[58]

$$\frac{t}{\lambda} = -\ln\left(\frac{I_0}{I_t}\right) = -\ln\,(T) \quad (1)$$

where I_0 is the zero-loss intensity, I_t is the total transmitted intensity, and sample thickness (t) is reported in units of the inelastic mean free path (λ), a measure known as "relative thickness." The electron transmission (T) can be taken as the ratio of zero-loss intensity to total intensity. From Fig. 5(b), the relative thickness of the TiN membrane is approximately 0.14. Multiplying this by the inelastic mean free path values reported for similar titanium-based ceramics[59] gives an estimated membrane thickness of 14 nm, which corroborates the thickness value of 10 nm calculated using ALD growth rates measured via ellipsometry.

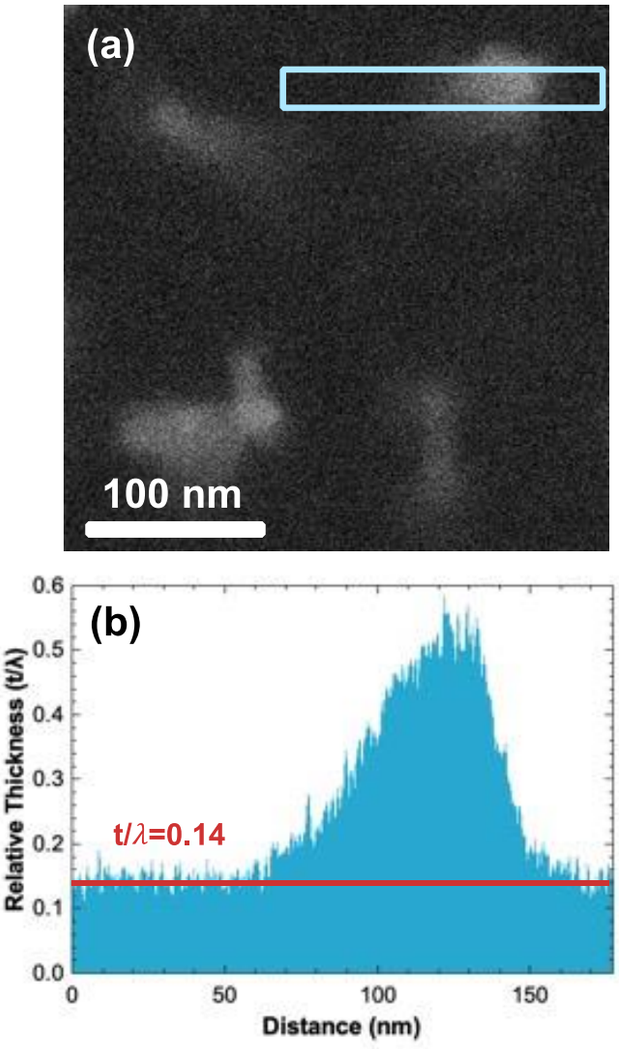

FIG. 5. A 10 nm thick TiN membrane was characterized with EELS using STEM imaging. (a) Spatial thickness map showing contamination on the membrane over an approximate 300 x 300 nm area. A line profile was taken over the area framed by the blue rectangle. (b) Line profile from the framed area, showing a relative thickness of 0.14 for the membrane.

The electron transparency of a membrane can be reported in terms of its electron transmission. Using the log-ratio formula above and the relative thickness of 0.14, the electron transmission of this membrane is approximately 0.87 at a 200 keV beam energy.

Dwyer and Harb[6] estimated the electron transmission of SiN windows from theoretical elastic scattering cross-sections developed by Riley et al.[60] for the 1–256 keV energy range. They report that for a 200 keV beam, a 10 nm thick SiN window has an estimated electron transmission of approximately 0.76, 14% lower than our measured value. This suggests that our 10 nm TiN membrane is more electron transparent than a SiN membrane of the same thickness, giving evidence to the successful fabrication of an isolated, ultra-thin membrane. Furthermore, this suggests that our membranes can compete with the current state-of-the-art in terms of electron transparency, demonstrating their viability as thin, electron-transparent sample supports for various characterization methods. This advantage over SiN is enhanced by the electrical conductivity of TiN, which can mitigate beam charging and enhance image resolution and contrast.[61] Four-point probe measurements taken on 55 nm thick TiN films deposited at 100°C gave a resistivity value of $6*10^{-5}$ ohm-m, similar to that of graphite (data in Supplemental Material).[62] To date, electron-transparent sample supports that are both electrically-conductive and made with scalable methods have not been reported in literature.

IV. CONCLUSION

We have described a novel nanofabrication process which can yield ultra-thin membranes from a variety of ALD-grown materials using a single flexible and scalable method. The process was used to fabricate TiN membranes 4 to 55 nm in thickness, characterization of which demonstrated electrical conductivity and a high electron transparency that can compete with SiN as the current state-of-the-art. Through our study of over-etching and residue removal, we show that the combination of support and

sacrificial materials used allows for a selective and convenient membrane release, without the need to perfect the final etch or tune it to the specific material being released. We have described the sources of residues on the back surface of the membrane and how to optimize the ALD deposition and backside release etches to prevent this.

We have demonstrated an advancement in the ability to fabricate ultra-thin membranes with greater flexibility and scalability with a process that enables the fabrication of highly-customized membranes with properties tuned to the needs of the application.

SUPPLEMENTAL MATERIAL

See supplementary material at [URL will be inserted by AIP Publishing] for ALD deposition parameters and four-point probe measurements for TiN resistivity.

ACKNOWLEDGMENTS

The authors would like to thank Hilary Brunner and Dominik Zeigler at Scuba Probe Technologies for running the Parylene-C depositions, Virginia Altoe for EDX analysis training and technical advice, Lauren Otto at Mekonos, Inc. for ellipsometry training and technical advice, and Karen Bustillo at the Molecular Foundry for technical advice.

Work at the Molecular Foundry was supported by the Office of Science, Office of Basic Energy Sciences, of the U.S. Department of Energy under Contract No. DE-AC02-05CH11231, as well as the Materials Sciences and Engineering Division of the U.S.

Department of Energy under Contract No. DE-AC02-05CH11231 within the in-situ TEM program (KC22ZH).

DATA AVAILABILITY

The data that supports the findings of this study are available within the article and its supplementary material. Additional data on ellipsometric and profilometry measurements for deposition and etch rates are available from the corresponding author upon reasonable request.

REFERENCES

[1]A. A. Barlian, W. T. Park, J. R. Mallon, A. J. Rastegar and B. L. Pruitt, P. IEEE **97** (3), 513-552 (2009).

[2]H. Nazemi, A. Joseph, J. Park and A. Emadi, Sensors **19** (6), 1285 (2019).

[3]P. Song, Z. Ma, J. Ma, L. Yang, J. Wei, Y. Zhao, M. Zhang, F. Yang and X. Wang, Micromachines **11** (1), 56 (2020).

[4]J. de Jong, R. G. H. Lammertink and M. Wessling, Lab Chip **6** (9), 1125-1139 (2006).

[5]A. Evans, A. Bieberle-Hütter, J. L. M. Rupp and L. J. Gauckler, J. Power Sources **194** (1), 119-129 (2009).

[6]J. R. Dwyer and M. Harb, Appl. Spectrosc. **71** (9), 2051-2075 (2017).

[7]L. Reimer and H. Kohl, *Transmission Electron Microscopy: Physics of Image Formation* (Springer New York, New York, NY, 2008), pp. 139-192.

[8]S. Franssila, *Introduction to Microfabrication*, 2nd ed. (John Wiley & Sons, Ltd, West Sussex, 2010).

[9] The Nanofab at University of Alberta, *KOH Etching of Bulk Silicon*, <https://www.nanofab.ualberta.ca/wp-content/uploads/downloads/2016/07/KOH-Etching-Info-2013_V2.pdf > (Accessed 5 Jul 2021).

[10]J. S. Bunch, S. S. Verbridge, J. S. Alden, A. M. van der Zande, J. M. Parpia, H. G. Craighead and P. L. McEuen, Nano Lett. **8** (8), 2458-2462 (2008).

[11]D. J. Kelly, M. Zhou, N. Clark, M. J. Hamer, E. A. Lewis, A. M. Rakowski, S. J. Haigh and R. V. Gorbachev, Nano Lett. **18** (2), 1168-1174 (2018).

[12]J. Yang, M. K. Choi, Y. Sheng, J. Jung, K. Bustillo, T. Chen, S.-W. Lee, P. Ercius, J. H. Kim, J. H. Warner, E. M. Chan and H. Zheng, Nano Lett. **19** (3), 1788-1795 (2019).

[13]S. M. George, Chem. Rev. **110** (1), 111-131 (2010).

[14]R. W. Johnson, A. Hultqvist and S. F. Bent, Mater. Today **17** (5), 236-246 (2014).

[15]O. Sneh, R. B. Clark-Phelps, A. R. Londergan, J. Winkler and T. E. Seidel, Thin Solid Films **402** (1), 248-261 (2002).

[16]Y. L. Mohammad Nasim, Ming Wen, Cuie Wen, J. Mater. Sci. Technol. **50** (0), 215-244 (2020).

[17]S. Vepřek, J. Vac. Sci. Technol. A **17** (5), 2401-2420 (1999).

[18]P. C. Yashar and W. D. Sproul, Vacuum **55** (3), 179-190 (1999).

[19]G. Chen, Phys. Rev. B **57** (23), 14958-14973 (1998).

[20]T. S. English, J. Provine, A. F. Marshall, A. L. Koh and T. W. Kenny, Ultramicroscopy **166**, 39-47 (2016).

[21]L. Gooseen, M.S. thesis, Delft University of Technology, 2018.

[22]Y. Lan, H. Wang, D. Wang, G. Chen and Z. Ren, J. Nanotechnol. **2010**, 279608 (2010).

[23]Y. H. Lu, C. Morales, X. Zhao, M. A. van Spronsen, A. Baskin, D. Prendergast, P. Yang, H. A. Bechtel, E. S. Barnard, D. F. Ogletree, V. Altoe, L. Soriano, A. M. Schwartzberg and M. Salmeron, Nano Lett. **20** (9), 6364-6371 (2020).

[24]K. Davami, L. Zhao, E. Lu, J. Cortes, C. Lin, D. E. Lilley, P. K. Purohit and I. Bargatin, Nat. Commun. **6** (1), 10019 (2015).

[25]V. Prodanović, H. W. Chan, H. V. D. Graaf and P. M. Sarro, Nanotechnology **29** (15), 155703 (2018).

[26]S. X. Tao, H. W. Chan and H. Van der Graaf, Materials **9** (12), 1017 (2016).

[27]H. van der Graaf, H. Akhtar, N. Budko, H. W. Chan, C. W. Hagen, C. C. T. Hansson, G. Nützel, S. D. Pinto, V. Prodanović, B. Raftari, P. M. Sarro, J. Sinsheimer, J. Smedley, S. Tao, A. M. M. G. Theulings and K. Vuik, Nucl. Instrum. Meth. A **847**, 148-161 (2017).

[28]J. Larkin, R. Henley, D. C. Bell, T. Cohen-Karni, J. K. Rosenstein and M. Wanunu, ACS Nano **7** (11), 10121-10128 (2013).

[29]K.-B. Park, H.-J. Kim, Y.-H. Kang, J.-S. Yu, H. Chae, K. Lee, H.-M. Kim and K.-B. Kim, Nanoscale **9** (47), 18772-18780 (2017).

[30]B. M. Venkatesan, B. Dorvel, S. Yemenicioglu, N. Watkins, I. Petrov and R. Bashir, Adv. Mater. **21** (27), 2771-2776 (2009).

[31]J. D. Baek, Y.-J. Yoon, W. Lee and P.-C. Su, Energ. Environ. Sci. **8** (11), 3374-3380 (2015).

[32]K. Kerman, T. Tallinen, S. Ramanathan and L. Mahadevan, J. Power Sources **222**, 359-366 (2013).

[33]J. H. Shim, C.-C. Chao, H. Huang and F. B. Prinz, Chem. Mater. **19** (15), 3850-3854 (2007).

[34]S. Goerke, M. Ziegler, A. Ihring, J. Dellith, A. Undisz, M. Diegel, S. Anders, U. Huebner, M. Rettenmayr and H.-G. Meyer, Appl. Surf. Sci. **338**, 35-41 (2015).

[35]L. Sainiemi, K. Grigoras and S. Franssila, Nanotechnology **20** (7), 075306 (2009).

[36]M. Berdova, T. Ylitalo, I. Kassamakov, J. Heino, P. T. Törmä, L. Kilpi, H. Ronkainen, J. Koskinen, E. Hæggström and S. Franssila, Acta Mater. **66**, 370-377 (2014).

[37]E. Österlund, J. Kinnunen, V. Rontu, A. Torkkeli and M. Paulasto-Kröckel, J. Alloys Compd. **772**, 306-313 (2019).

[38]V. Rontu, A. Nolvi, A. Hokkanen, E. Haeggström, I. Kassamakov and S. Franssila, Mater. Res. Express **5** (4), 046411 (2018).

[39]L. Wang, J. J. Travis, A. S. Cavanagh, X. Liu, S. P. Koenig, P. Y. Huang, S. M. George and J. S. Bunch, Nano Lett. **12** (7), 3706-3710 (2012).

[40]K. R. Williams, K. Gupta and M. Wasilik, J. Microelectromech. S. **12** (6), 761-778 (2003).

[41]W. Lengauer, S. Binder, K. Aigner, P. Ettmayer, A. Guillou, J. Debuigne and G. Groboth, J. Alloys Compd. **217** (1), 137-147 (1995).

[42]D. S. Stone, K. B. Yoder and W. D. Sproul, J. Vac. Sci. Technol. A **9** (4), 2543-2547 (1991).

[43]B. Elsener, A. Rota and H. Böhni, Mater. Sci. Forum **44**, 29-38 (1989).

[44]M. Birkholz, K.-E. Ehwald, P. Kulse, J. Drews, M. Fröhlich, U. Haak, M. Kaynak, E. Matthus, K. Schulz and D. Wolansky, Adv. Funct. Mater. **21** (9), 1652-1656 (2011).

[45]D. R. Ciarlo, Biomed. Microdevices **4** (1), 63-68 (2002).

[46]A. W. Grant, Q. H. Hu and B. Kasemo, Nanotechnology **15** (9), 1175-1181 (2004).

[47]W. W. Molzen, A. N. Broers, J. J. Cuomo, J. M. E. Harper and R. B. Laibowitz, J. Vac. Sci. Technol. **16** (2), 269-272 (1979).

[48]W. F. Gorham, J. Polym. Sci. A1 **4** (12), 3027-3039 (1966).

[49]J. Ortigoza-Diaz, K. Scholten, C. Larson, A. Cobo, T. Hudson, J. Yoo, A. Baldwin, A. Weltman Hirschberg and E. Meng, Micromachines **9** (9), 422 (2018).

[50]R. P. von Metzen and T. Stieglitz, Biomed. Microdevices **15** (5), 727-735 (2013).

[51]K. R. Williams, J. Therm. Anal. **49** (2), 589-594 (1997).

[52]P. K. Wu, G. R. Yang, J. F. McDonald and T. M. Lu, J. Electron. Mater. **24** (1), 53-58 (1995).

[53]V. Miikkulainen, M. Leskelä, M. Ritala and R. L. Puurunen, J. Appl. Phys. **113** (2), 021301 (2013).

[54]O. M. E. Ylivaara, X. Liu, L. Kilpi, J. Lyytinen, D. Schneider, M. Laitinen, J. Julin, S. Ali, S. Sintonen, M. Berdova, E. Haimi, T. Sajavaara, H. Ronkainen, H. Lipsanen, J. Koskinen, S.-P. Hannula and R. L. Puurunen, Thin Solid Films **552**, 124-135 (2014).

[55]J. I. Goldstein, D. E. Newbury, P. Echlin, D. C. Joy, C. E. Lyman, E. Lifshin, L. Sawyer and J. R. Michael, *Scanning Electron Microscopy and X-ray Microanalysis: Third Edition* (Springer US, Boston, MA, 2003), pp. 297-353.

[56]K. Kanaya and S. Okayama, J. Phys. D: Appl. Phys. **5** (1), 43-58 (1972).

[57]J. F. Moulder and J. Chastain, *Handbook of X-ray Photoelectron Spectroscopy: A Reference Book of Standard Spectra for Identification and Interpretation of XPS Data*. (Physical Electronics Division, Perkin-Elmer Corporation, Eden Prairie, 1992).

[58]T. Malis, S. C. Cheng and R. F. Egerton, J. Electron Micr. Tech. **8** (2), 193-200 (1988).

[59]H. Shinotsuka, S. Tanuma, C. J. Powell and D. R. Penn, Surf. Interface Anal. **51** (4), 427-457 (2019).

[60]M. E. Riley, C. J. MacCallum and F. Biggs, Atom. Data Nucl. Data Tables **15** (5), 443-476 (1975).

[61]J. Cazaux, Ultramicroscopy **60** (3), 411-425 (1995).

[62]D. C. Giancoli, *Physics : principles with applications*. (Prentice-Hall, Englewood Cliffs, 1995).

Journal of Vacuum Science Technology B

PLEASE CITE THIS ARTICLE AS DOI: 10.1116/6.0001309

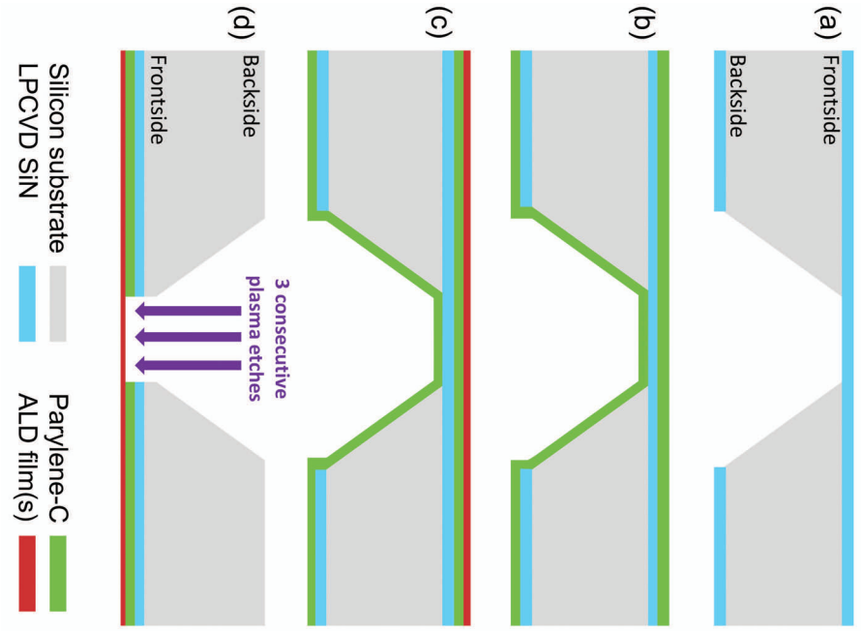

Journal of Vacuum Science Technology B

PLEASE CITE THIS ARTICLE AS DOI: 10.1116/6.0001309

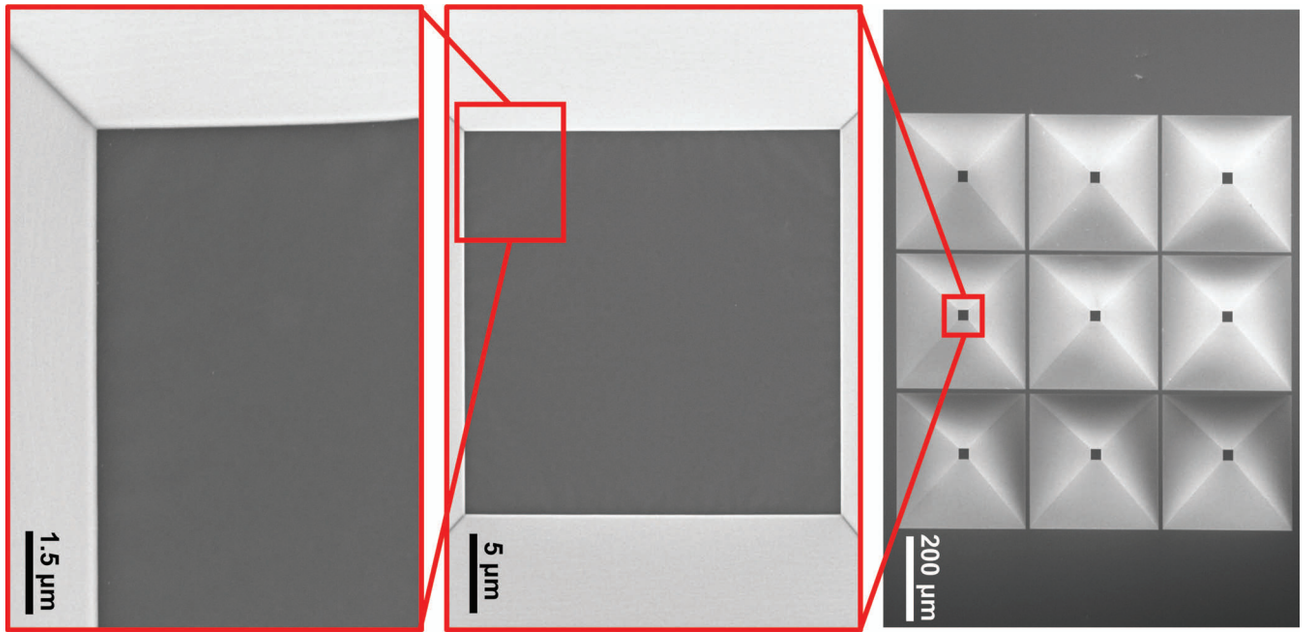

Journal of Vacuum Science Technology B

PLEASE CITE THIS ARTICLE AS DOI: 10.1116/6.0001309

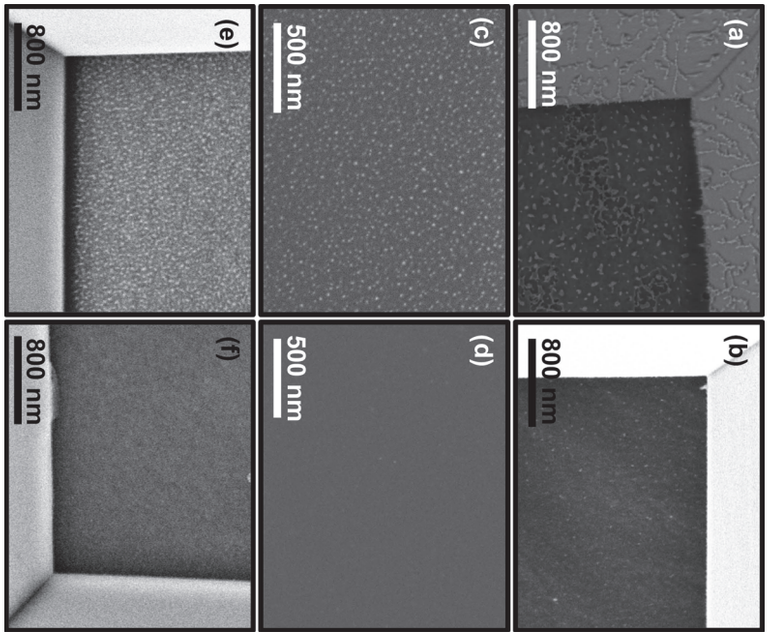

Journal of Vacuum Science Technology B

PLEASE CITE THIS ARTICLE AS DOI: 10.1116/6.0001309

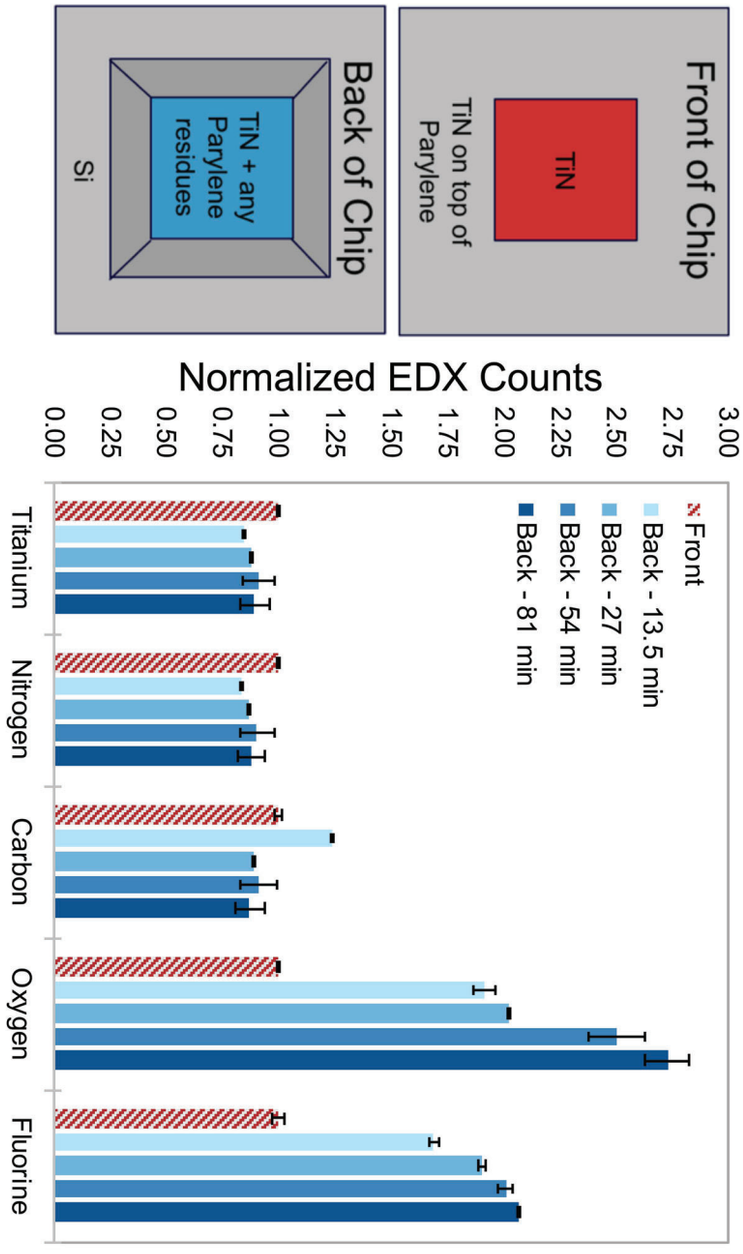

Journal of Vacuum Science Technology B

PLEASE CITE THIS ARTICLE AS DOI: 10.1116/6.0001309